

Article

Study on the Mechanical Properties of Polyurethane-Cement Mortar Containing Nanosilica: RSM and Machine Learning Approach

M. S. M. Al-kahtani ¹, Han Zhu ^{1,2,*}, Yasser E. Ibrahim ^{3,*} , S. I. Haruna ³ and S. S. M. Al-qahtani ¹

- ¹ School of Civil Engineering, Tianjin University, Tianjin 300350, China; aboothman2012@hotmail.com (M.S.M.A.-k.); sagralqahtani7747@gmail.com (S.S.M.A.-q.)
- ² Key Laboratory of Coast Civil Structure Safety of the Ministry of Education, Tianjin University, Tianjin 300350, China
- ³ Engineering Management Department, College of Engineering, Prince Sultan University, Riyadh 11586, Saudi Arabia; sharuna@psu.edu.sa
- * Correspondence: hanzhu2000@tju.edu.cn (H.Z.); ymansour@psu.edu.sa (Y.E.I.)

Abstract: Polymer-modified cement mortar has been increasingly used as a runway/road pavement repair material due to its improved bending strength, bonding strength, and wear resistance. The flexural strength of polyurethane–cement mortar (PUCM) is critical in achieving a desirable maintenance effect. This study aims to evaluate and optimize the flexural strength of PUCM involving nano silica (NS) using a central composite design/response surface methodology (CCD/RSM) to design and establish statistical models. The PU binder and NS were utilized as input parameters to evaluate the responses, such as compressive and flexural strength. Moreover, machine learning (ML) algorithms including artificial neural networks (ANN) and Gaussian regression process (GPR) were used. The PUCM mixtures were prepared by adding a PU binder at 0%, 10%, 15%, and 25% by weight of cement. At the same time, NS was incorporated into the mortar mixes at 0 to 3% (interval of 1%) by cement weight. The results showed that the simultaneous effect of PU binder at the optimal content and NS improved the performance of PUCM. Adding NS to the mortar mixture mitigated some of the strength lost due to the PU binder, which remarkably reduces the strength properties at a high content. The optimized PUCM can be obtained by partly adding 3.5% PU binder and 2.93% NS particles by the weight of cement. The performance of the machine learning algorithms was tested using performance indicators such as the determination of coefficient (R^2), mean absolute error (MAE), mean-square error (MSE), and root-mean-square error (RMSE). The GPR algorithm outperformed the ANN with higher R^2 and lower MAE values in the training and testing phases. The GPR can predict flexural strength with 90% accuracy, while ANN can predict it with 75% accuracy.

Keywords: mortar; polyurethane; response surface methodology; artificial intelligent; mechanical properties



Citation: Al-kahtani, M.S.M.; Zhu, H.; Ibrahim, Y.E.; Haruna, S.I.; Al-qahtani, S.S.M. Study on the Mechanical Properties of Polyurethane-Cement Mortar Containing Nanosilica: RSM and Machine Learning Approach. *Appl. Sci.* **2023**, *13*, 13348. <https://doi.org/10.3390/app132413348>

Academic Editor: Jong Wan Hu

Received: 29 October 2023

Revised: 18 November 2023

Accepted: 15 December 2023

Published: 18 December 2023



Copyright: © 2023 by the authors. Licensee MDPI, Basel, Switzerland. This article is an open access article distributed under the terms and conditions of the Creative Commons Attribution (CC BY) license (<https://creativecommons.org/licenses/by/4.0/>).

1. Introduction

Concrete is a commonly used construction material [1], which exhibits high performance and good durability. But, it is brittle and characterized by weak tensile strength, resulting in easy crack formation when subjected to flexural loading [2]. Moreover, ordinary concrete reveals weak deformability and low compression toughness, affecting its ability to resist dynamic loads. These shortcomings limit the application of concrete in some civil engineering structures prone to impact loads, like mechanical platforms and airport pavement, often subjected to repetitive loads in their service life. Many studies have been carried out to improve such desired concrete properties to overcome these shortcomings [3,4]. Polyurethane polymer material is proving to be a potential candidate to enhance

concrete properties such as durability, impact resistance, and water absorption capacity, as found in the literature [5–7], required for engineering structure and maintenance purposes.

The damage in civil engineering structures results from several factors, such as corrosion due to aggressive environments, the use of de-icing salts, high chloride levels in the air, the alkali effect, and poor design or construction. Moreover, concrete cracking usually complements steel corrosion, resulting in a decreased load-carrying capacity of the structure [5,8]. Polymer concrete has been applied to maintain damaged concrete members, such as industrial flooring, underground pipes, and road pavement, where high strength, durability, and a fast setting are desirable [9]. The polymer comprises several thousand repetitive units in their extremely long molecules. These include rubber, Polyethylene (PE), Epoxy Resins, Polyurethane (PU), and other polymer materials [10–13]. Due to its desirable properties, PU has attracted the attention of researchers among these polymeric materials to carry out studies on PU-based polymer materials [7,14,15], a PU–cement composite [5,6], elastomeric polymer material [16], polymer-modified bitumen [17], coating material [18], grouting materials [19], and polyurethane foams [20,21]. Compared with ordinary polymer materials, PU demonstrates a high resistance to chemical attacks, good adhesion, fast hardening, and great mechanical properties, capable of enhancing the cementitious material toughness with a low content [5,22]. It is widely used in pavement structures due to its excellent performance [12,14]. A PU-cement based composite was obtained by adding polyurethane binder into cementitious material such as concrete and mortar, which helps maintain and rehabilitate engineering structures [23].

The mechanical properties of PU-cement based composite have been studied by [23–25]. Hussain et al. [5] investigated PU-based cement's bonding strength and mechanical behavior as a repair material for existing bridges. The result showed that the mechanical properties and density were improved from 400 kg/m³ to 1650 kg/m³, and PUC demonstrates high bond properties with cement-based materials. Harith [23] reported that PU foam decreases mechanical behavior and improves shrinkage performance. Tang et al. [26] reported that cation PU accelerates the hydration of cement, modifies its mineral content, and decreases cement's brittleness. Moreover, the inclusion of a 0.5% PU content improved the tensile property at early age of curing time. Chen et al. [27] introduced nano silica as a filler material in polymer nanocomposite for the improvement in mechanical properties.

In the last decade, conventional linear and nonlinear analyses have been employed to evaluate the properties of concrete. For instance, the design of the experiment and regression analysis was used to determine concrete behavior and optimize the concrete mixtures. However, these conventional techniques have some deficiencies when dealing with complex problems. Previous studies have indicated that artificial intelligence has been used in engineering applications to solve complex problems. These include artificial neural networks [28,29] emotional intelligence and traditional FFNNs [30], novel data intelligent algorithms [31], the Hammerstein–Wiener and SVM models [32], ANNs, K-nearest neighbor, regression tree, and Multi-response optimization [28,33] being adopted. Lee et al. [34] evaluated the performance of credit scoring from the mining data techniques using classification, regression trees, and adaptive regression splines. Chou and Tsai [35] analyzed the compressive strength of high-performance concrete using classification and regression techniques. Kooshkaki et al. [36] used a multi-objective ANN model to analyze the porosity on the prediction of hardening behavior of mortar involving micro and nano-silica. The results showed that concrete flexural strength was estimated with high accuracy. Ayaz et al. [37] established artificial neural networks, decision trees, and gradient-boosting models to predict concrete properties subjected to high temperatures. Rupasinghe et al. [38] used a multiscale approach to estimate the strength of nano-engineered concrete involving nano-silica.

Moreover, several studies have attempted to analyze the hardened behavior of polyurethane cement concrete using conventional and artificial intelligence techniques. Few studies have been performed so far concerning polyurethane–cement concrete. For instance, Gao and Sun [39] proposed a combined theoretical deduction and experimental

method to predict the fatigue life of a polyurethane cement composite subjected to low and high temperatures. The authors reported that the proposed formula could effectively evaluate polyurethane cement composites' fatigue life and limit. Diaconescu et al. [40] used the ANN algorithm to study the effect of powdered tire waste and the epoxy resin content on the mechanical properties of polymer concrete. Marinela et al. [41] developed an ANN model for the prediction of mechanical properties (compressive and flexural strength) of polymer concrete containing fly ash. The polymer concrete containing different fly ash and resin contents was tested to evaluate the effect of fly ash on the strength.

PU-cement mortar has been widely used as a repair material for civil engineering infrastructure such as concrete buildings and pavement. However, previous [6,26,42] studies have indicated that PU binder negatively affects cementitious material by reducing mechanical properties. On the other hand, nanosilica improves the mechanical properties of cementitious materials (mortar and ordinary concrete) by reducing pore structures, thus densifying the materials, which leads to the improvement in mechanical properties [43,44], was incorporated into the PU-cement mortar in this study, targeting the mitigation of the negative effect PU binder in the mortar. Therefore, the main aim of this study was to comprehensively evaluate the mechanical properties of PU-cement mortar incorporated with nanosilica. The RSM/CCD model was employed to optimize mortar mixtures and evaluate the mechanical properties. On the other hand, machine learning (ML) algorithms such as ANN and GPR were used to predict the flexural strength. The prediction skill of ML algorithms was then compared with the RSM model.

2. Materials and Methods

2.1. Materials

The PUCM mixtures were prepared using Grade 42.5R cement, and the chemical properties of the cement are summarized in Table 1. The river sand was utilized as the fine aggregate, with a fineness modulus of 2.08, and its apparent density was 2626 kg/m^3 , with a maximum particle size of 2.26 mm. The particle size distribution curve is depicted in Figure 1. The PUCM was prepared with a polycarboxylate-based superplasticizer characterized by a 20% water reducer introduced at 0.15% by cement weight to achieve better performance.

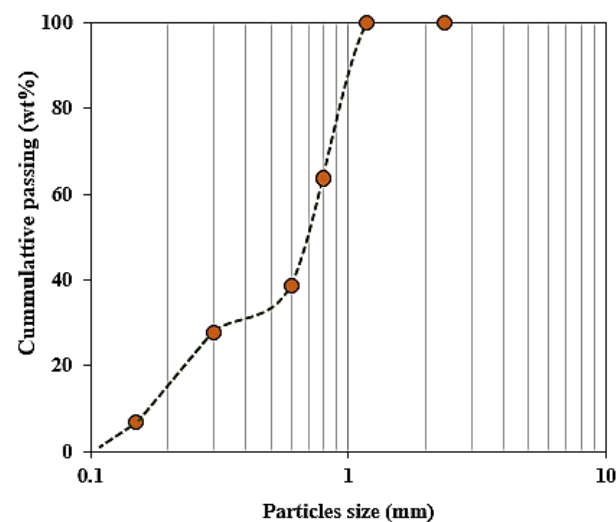


Figure 1. Particle distribution curve of aggregates used.

Table 1. Chemical compositions of cement.

Material	Oxides									
	SiO ₂	Al ₂ O ₃	Fe ₂ O ₃	CaO	MgO	K ₂ O	Na ₂ O	SO ₃	TiO ₂	LOI
Cement	23.270	4.410	2.450	62.850	1.420	0.480	0.210	2.570	0.080	1.820

PU Binder

The polymerization reaction between diol (involving two or more hydroxyl –OH groups) and isocyanate (involving two or more isocyanate –NCO groups) produced a PU binder [45]. It is a type of polymer with broad applications in civil engineering structures due to its excellent performance, such as elastic modulus and elongation at break. The physical indexes of the PU binder are presented in Table 2. The PU binder was produced by mixing polyol (mixture of castor oil and CaCO₃) as the main chemical composition with polymethylene polyphenylene isocyanate (PAPI) involving the diisocyanate group (–NCO), using a mixing ratio of 6:1 by weight, and carefully mixed in a container at room temperature.

Table 2. Indexes of PU binder.

PU Binder	Viscosity (CPS)	Appearance	Curing Age (h)		Tension Property (MPa)
			Initial	Final	
Polyol	35,000	Grey white sticky	-	-	-
PAPI	250	Brown transparent	-	-	-
PU binder	-	-	3.5	72	5.5

2.2. Mix Proportion and Specimen Preparation

Table 3 summarizes the mixed proportion of PUCM modified with NS. A total of 13 groups of PU–cement mortar containing different PU binders and NS content were prepared in this study. The PU binder was introduced to the cement mortar mixtures by cement weight at 0%, 10%, 15%, and 25%, while NS was introduced into the mortar mixture also by the weight of cement at 0 to 3% (interval of 1%) as summarized in Table 3. The constant water-to-cement (w/c) ratio of 0.25 was used to prepare all PU-modified cement mortar mixtures.

Table 3. Mix proportion of the mortar material (1 kg/m³).

S/N	Mixture ID	Cement	PU Binder	NS	Sand	Water	Superplasticizer
1	PUCM0-0	702	0.00	0.00	1404	175.5	14.04
2	PUCM10-0	702	70.2	0.00	1404	175.5	14.04
3	PUCM10-1	702	70.2	7.02	1404	175.5	14.04
4	PUCM10-2	702	70.2	14.04	1404	175.5	14.04
5	PUCM10-3	702	70.2	21.06	1404	175.5	14.04
6	PUCM15-0	702	105.3	0.00	1404	175.5	14.04
7	PUCM15-1	702	105.3	7.02	1404	175.5	14.04
8	PUCM15-2	702	105.3	14.04	1404	175.5	14.04
9	PUCM15-3	702	105.3	21.06	1404	175.5	14.04
10	PUCM25-0	702	175.5	0.00	1404	175.5	14.04
11	PUCM25-1	702	175.5	7.02	1404	175.5	14.04
12	PUCM25-2	702	175.5	14.04	1404	175.5	14.04
13	PUCM25-3	702	175.5	21.06	1404	175.5	14.04

The mortar containing PU binder modified with NS were produced based on the following steps: firstly, the dry materials, which includes sand, cement, and NS were placed in an SJ-15 cement mortar mixer and mixed thoroughly for 1 min with a slow speed. Then,

water containing superplasticizer was introduced to the dry mix and continued mixing for another 2 min. Subsequently, freshly prepared PU binders with various contents were introduced to the mortar mixes and we continued mixing until a homogeneous cement mortar mixture was achieved. Therefore, three specimens from each group were cast using prismatic specimens of a $40 \times 40 \times 160 \text{ mm}^3$ mold to evaluate mechanical properties. After 24 h, the beam specimens were de-molded and kept in the standard curing room (temperature = $20 \pm 2 \text{ }^\circ\text{C}$ and relative humidity $\geq 99\%$) for 28 days before the testing. To achieve more reliable results, three samples from each PUCM sample were tested, and their average was measured as the test result. Figure 2 illustrates the systematic process of PUCM mixture and testing method.

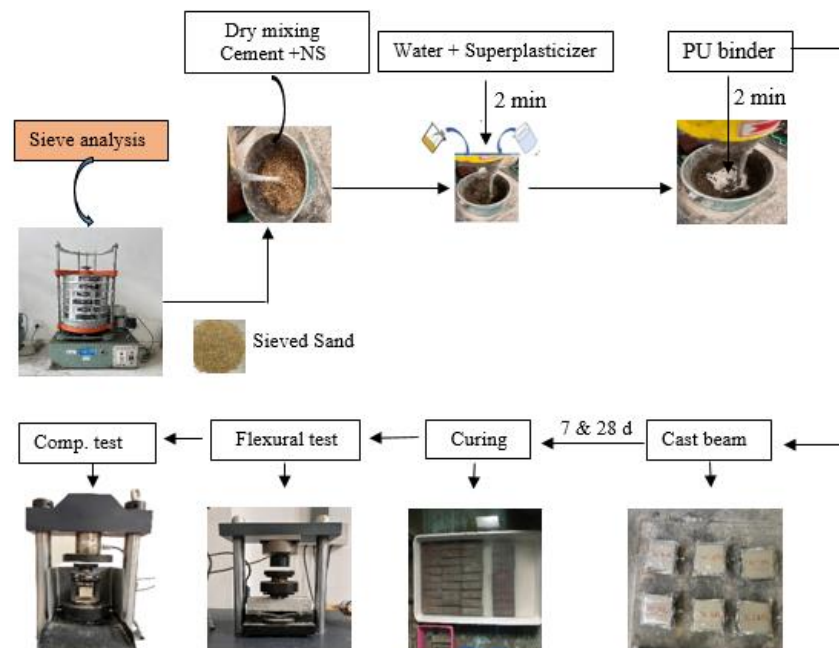


Figure 2. Systematic illustration of the mixing process and testing program.

2.3. Methods

Mechanical Properties Test

The PUCM mechanical qualities were tested following DL/T5126-2001 [46]. For each mixing condition, prismatic specimens of $40 \times 40 \times 160 \text{ mm}^3$ were tested utilizing a 3-point flexural load. The prism specimens were positioned on two equal supports with a defined span of 100 mm. Compression testing was performed after dividing the flexural test samples into two pieces. The mechanical properties tests were conducted using UTM, which has a 30 tons capacity and is set at speed rates of 50 N/s for the flexural and 2.4 kN/s for the compressive strength test.

2.4. Response Surface Methodology

RSM is a mathematical method commonly used to evaluate and establish a model for a dataset containing independent and dependent variables. In addition, RSM has been applied in multi-objective optimization models that try to accomplish desired objectives according to either predicted or input parameters [47]. Many models can be employed in RSM modeling to establish statistical connections between independent variables and the target variable. These consist of the historical data model, Box–Behnken, central composite design (CCD) model, etc. The number of variables and degree of variability determine the model type for analysis [47]. If the relationship between the input parameter and output is uncertain, a linear function could be constructed using the first-order expression, as given in Equation (1). Figure 3 illustrates the CCD framework according to four points, displaying factorial points (± 1) and four central points describing ($\pm\alpha$) design points. The

experimental dataset from thirteen (13) mixes was prepared with combination of three levels of variables (PU binder and NS) that were used to analyze the CCD model due to its flexibility for selecting α (distance from design center to axial run); $\alpha = 1$ was implemented in this study [47]. According to Equations (1) and (2), the input parameters and output responses were statistically stated in a linear or polynomial form, respectively [47].

$$r = \beta_0 + \beta_1 X_1 + \beta_2 X_2 + \dots + \beta_n X_n + \epsilon \tag{1}$$

However, for non-linear interactions in the dataset, a higher-degree polynomial model, the second-order function stated in Equation (2), can be utilized:

$$r = \beta_0 + \sum_{i=1}^k \beta_i X_i + \sum_{i=1}^k \beta_{ii} X_i^2 + \sum_{i < j} \beta_{ij} X_i X_j + \epsilon \tag{2}$$

where r is the output, β_0 is the r-intercept, in which $X_1 = X_2 = 0$, β_1 is the coefficient of first input parameter, β_2 is the coefficient of the second input parameter, X_1 and X_2 are the first and second input parameter coefficients, ϵ represents the error, i and j are the linear and quadratic coefficient, and k is the variable number [47].

The CCD was utilized for model analysis to optimize the response variable. Therefore, a PU binder content of 0%, 10%, 15%, or 25% was added to the mortar mixture based on the cement weight, and NS was also added to the mortar from 0 to 3% (intervals of 1%) by cement weight, and they were modeled as input parameters.

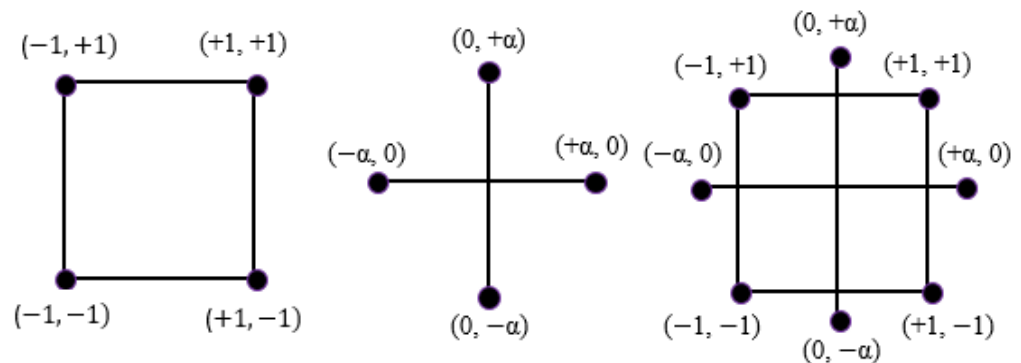


Figure 3. CCD framework.

2.5. Artificial Intelligence-Based Model

2.5.1. ANN

The ANN is a modeling algorithm used in data analysis that employs a decision-layer network. This model is made up of processing components linked together by synaptic weight or neurons. As seen in Figure 4, an input, hidden, and an output layer comprises the model structures. The inputs are multiplied by a modified weight and then sent via a transfer function to generate the neurons' output [48]. As a result of the network's training of the dependent and independent parameters, the best weight is computed through learning practice. The neurons in Figure 4 collect the input parameters, and the Net is the total of computed weight and bias in each neuron [49], and expressed in Equation (3):

$$Net = \sum_{i=1}^n w_{ij} x_i + b_i \tag{3}$$

The hyperbolic tangent function was used for better prediction skills. It has function values from -1 to 1 , and it is given in Equation (4):

$$y = f(Net) = \frac{2}{1 + e^{-2.net}} - 1 \tag{4}$$

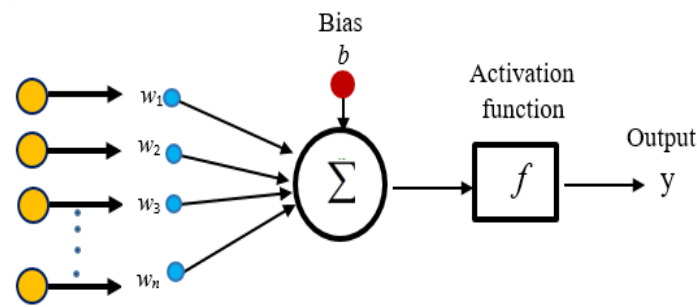


Figure 4. Architecture of the ANN model.

2.5.2. GPR

GPR is a probabilistic, nonparametric, reliable nonlinear prediction model, supervised, and unsupervised learning technique that uncovers nonlinear and complicated function mapping concealed in datasets. GPR has recently drawn more research interest from engineers across all engineering disciplines [50,51]. Kernel functions are used in GPR to handle nonlinear data. Furthermore, the GPR model’s ability to respond accurately to the input parameter is one of its benefits [52]. The modelling procedure is depicted in Figure 5.

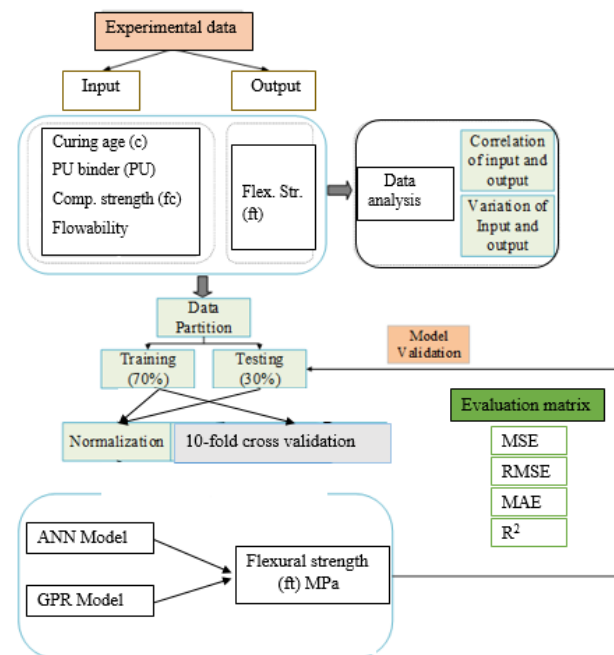


Figure 5. The methodology of the developed model.

For a training set $K = \{(z_i, y_i) | i = 1, \dots, n\}$ the input data $Z \in R^{K \times n}$ is known as the design matrix, and $y \in R^n$ is the vector of the target output. The major assumption of the GPR model is that the predicted y is determined as [53]

$$y = f(z) + \varepsilon \tag{5}$$

where $\varepsilon \sim N(0, \sigma_n^2)$, $\varepsilon \in R$ is the homoscedastic noise of the all samples z_i .

For the GPR model, the n observation in the dataset of interest $y = \{y_1, \dots, y_n\}$ is regarded as a one-point sample from a multivariate Gaussian distribution (GD).

2.6. Hyperparameter Turning and Cross-Validation

The operation and structures of the learning process of AI techniques were controlled by hyperparameters, as depicted in Figure 6. It was considered the best way to improve the estimation accuracy of the developed model. Therefore, the random search (RS) method

was adopted to tune the ML algorithm of hyperparameters, which outperformed the firefly algorithm [39,40] and was adopted in this study. Cross-validation was used to control the model and applied when tuning hyperparameters for small datasets. Moreover, tenfold validation was also adopted in our work. The experimental dataset was proportioned to 70 for training and 30 for testing.

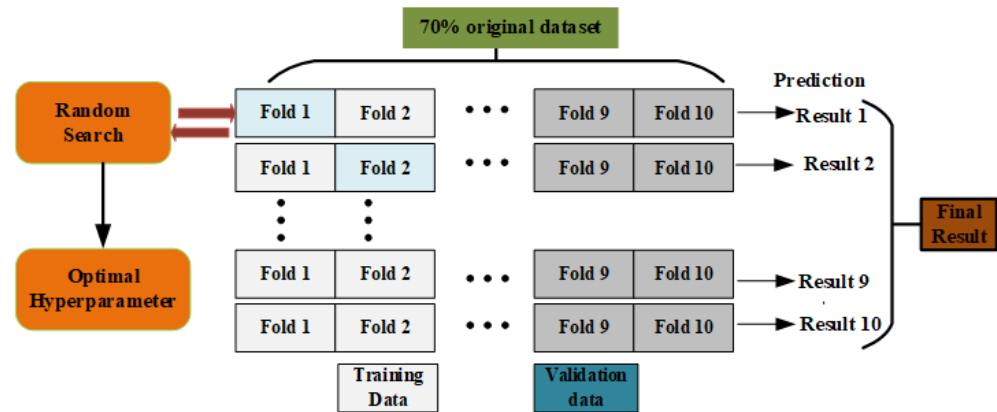


Figure 6. Hyperparameter tuning process.

2.7. Performance Evaluation

Five evaluation matrices were utilized in this study to determine the performance of the established ML algorithms. The matrices included the MSE, RMSE, MAE, R², and R. Additionally, Table 4 summarizes the expression equation for each matrix. The *m_i* and *p_i* are the measured and predicted values, respectively; *p* is the number of input variables, and *n* is the number of observations.

Table 4. Evaluation matrices.

Matric	Equation	Description
R ²	$\left[\frac{\sum_{i=1}^n (m_i - \bar{m})(p_i - \bar{p})}{\sqrt{\sum_{i=1}^n (m_i - \bar{m})^2 \sum_{i=1}^n (p_i - \bar{p})^2}} \right]^2$	R ² is a commonly used performance metric to describe how well a model predicts a given variable. Its value ranges from 0 to 1. When R ² is near to 1, high prediction accuracy is attained [54,55].
MSE	$\frac{1}{n} \sum_{i=1}^n (m_i - \bar{m}_i)^2$	The statistical error demonstrating the model’s performance. The MSE value was very near to zero, which indicates excellent prediction accuracy.
RMSE	$\sqrt{\frac{1}{n} \sum_{i=1}^n (m_i - p_i)^2}$	The difference between the predicted value and the observed value is indicated by RMSE. When the RMSE value approaches 0, better performance is achieved.
MAE	$\frac{1}{2} \sum_{i=1}^n m_i - p_i $	MAE revealed the mean absolute error value between the predicted and observed value. It has a range between 0 < MAE < ∞.

3. Results and Discussions

3.1. Compressive Strength of PU–Cement Mortar

Figure 7 shows the compressive strength of the PU–cement mortar containing nano silica. The average compressive strength of the control mortar (PUCM0-0) at 28 d curing age was 60.28 MPa. All PU–cement-modified specimens revealed a decrease in compressive strength due to adding the PU binder. As depicted in Figure 7, the addition of 10% PU binder without NS led to a decrease in strength of 22.81%. However, the rate of strength reduction was mitigated due to the reinforcing effect of the NS particles at various contents, as noted in PUCM10-1, PUCM10-2, and PUCM10-3, which reduced by 19.81%, 15.56%, and 17.44%, respectively, compared to the reference sample. The result indicated that the addition of the NS material mitigated some of strength lost due to the PU binder. This finding agreed with previous studies [43,44], which showed that NS improves the compressive strength of mortar, and the improvement mechanism is due to the filling of

pore structure in the cement mortar and promotes the hydration process of the matrix. Additionally, a further decrease in the compressive strength was noted in the PU–cement mortar containing 15% PU binder. The PUCM15-0 revealed a compressive strength of 41.52 MPa, which was 31.51% lower than the control specimen (PUCM0-0). Similarly, a remarkable reduction in the compressive strength of the PU-cement mortar was noted in the specimens involving the highest PU binder content (25% PU binder), as revealed in the PUCM25-0 specimen with 31.34 MPa, which appeared to be the lowest strength recorded among all mixes. This strength was improved due to the addition of NS, as demonstrated in PUCM25-1, PUCM25-2, and PUCM25-3. This indicates the reinforcing effect of NS. In spite of the negative effect of PU binder content when added in lower and higher content, NS particles were able to mitigate some of the strength loss due to the introduction of the polymer materials.

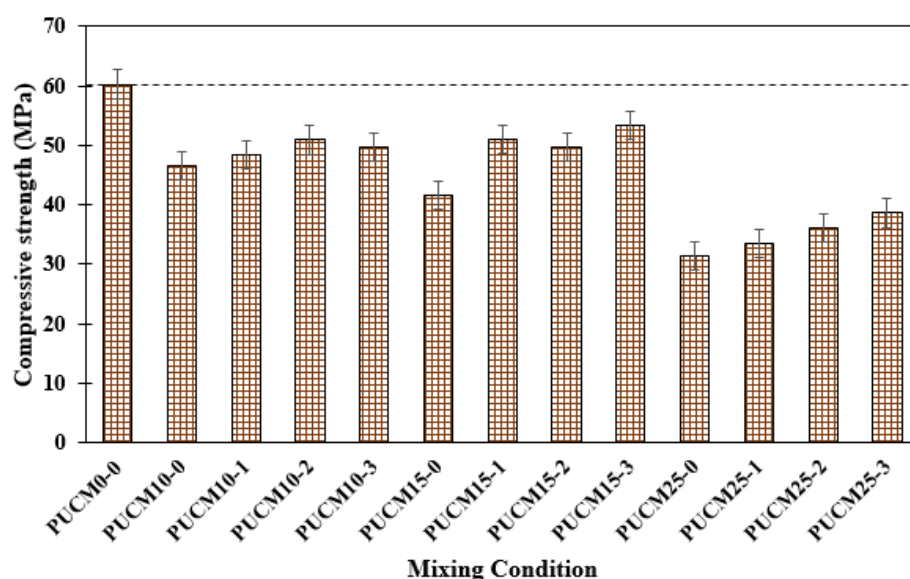


Figure 7. Compressive strength of PUCM modified with nano silica.

Previous research has indicated that the polyurethane binder significantly decreases the mechanical properties, particularly the compressive strength of cement-based composites, as reported in the literature [6,26,42]; the strength decreases with the increase in PU binder content. The reduced strength is attributed to the cement particles' adsorption to reduce the mixtures' hydration process and the formation of more void in the cement mortar. However, the incorporation of PU binder in the cement-based composite improved the desirable performance of durability-related properties such as water absorption, early and long-term shrinkage, etc. Due to its viscoelastic behavior, the influence of PU binder prevents crack propagation in cement-based materials [56].

3.2. Flexural Strength of PU–Cement Mortar

The flexural strength of PU–cement mortar modified with or without NS particles is shown in Figure 8. The flexural strength of the control mortar (PUCM0-0) is 12.96 MPa. Adding 10% PU without NS led to an increase in strength of 6.17%. Under the same 10% PU content and reinforced with NS, the flexural strength revealed improved strength, as indicated in PUCM10-1, PUCM10-2, and PUCM10-3 specimens. This behavior is attributed to the combined effect of PU binder and NS in improving the flexural strength of cement-based composites. The positive effect of PU binder agrees with findings in the past literature [6,26]; the viscoelastic properties of PU binder are responsible for this behavior. Due to the addition of 10% PU binder and 2% NS and 3% NS, the flexural strength was increased by 8.88% and 16.69%, respectively. Similarly, the reinforcing effect of NS was also noted in the specimens containing 15% PU binder. A moderate PU binder content obviously

improved cement mortar’s flexural strength. The average flexural strength of PUCM15-0 was 14.10 MPa which is 8.79% higher than the reference specimen. For the specimens prepared with 15% PU, the flexural strength decreased and then increased with an increase in NS particles. PUCM15-3 demonstrated the highest strength of 14.77 MPa among this group. The higher PU binder content also negatively affects the flexural strength, as shown in Figure 8. All the specimens containing 25% PU revealed a reduced flexural strength compared to others. The flexural strength of PUCM25-0 was 11.34 MPa, and appeared to be the lowest strength among all the specimens. However, some of the lost strength was mitigated due to the reinforcing effect of NS, as revealed in the PUCM25-1, PUCM25-2, and PUCM25-3 specimens.

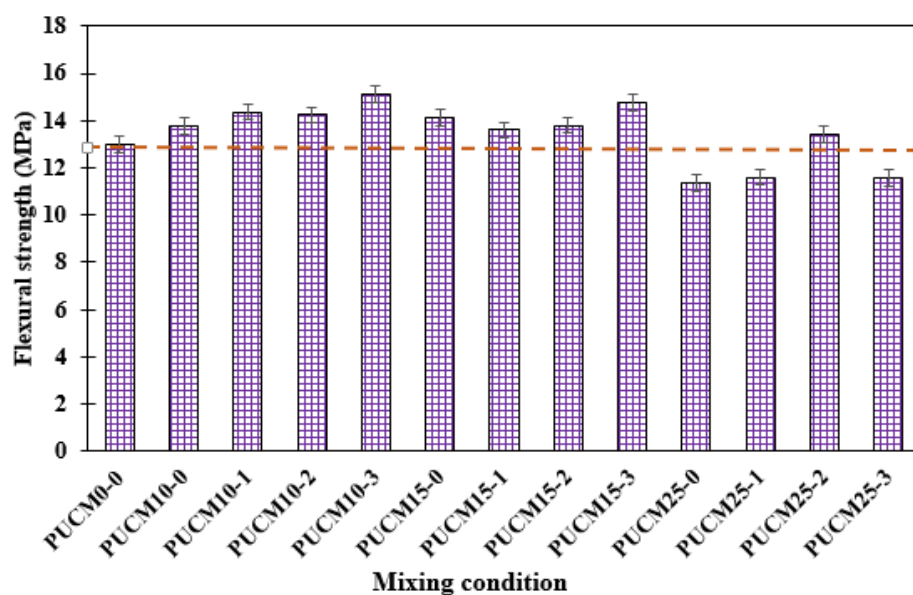


Figure 8. Flexural strength of PUCM modified with nano silica.

3.3. Result of RSM/CCD Analysis

Table 5 shows the developed RSM analysis involving the independent parameters (PU binder and NS) and response parameters, including compressive strength and flexural strength, demonstrating the model combination. Therefore, the ANOVA was used to determine the significance and variability of the established model, as indicated in Table 5.

Table 5. Coded model combination for developed CCD analysis.

Run	Coded Value		Responses	
	PU Binder	NS	Flexural Strength (MPa)	Compressive Strength (MPa)
1	0	0	13.8	49.77
2	0	0	13.8	49.77
3	−1	1	15.13	49.77
4	−1	0	14.23	50.9
5	0	1	14.77	53.36
6	0	−1	13.6	51.06
7	0	0	13.8	49.77
8	−1	−1	11.6	33.5
9	0	0	13.8	49.77
10	1	1	11.57	38.63
11	1	0	13.34	36.1
12	1	−1	11.34	33.5
13	0	0	13.8	49.77

3.3.1. ANOVA Result

The ANOVA of the cubic models developed from the RSM/CCD model is summarized in Table 6. The established model *F*-values of 5.04 and 12.75 were obtained for the flexural and compressive strength model, respectively, revealing the significance of the model with a *p*-value of 0.0468 for the flexural strength and 0.0064 for the compressive strength. The significance of the models and related terms was checked using a 95% confidence level (i.e., *p*-value < 0.05). As shown in Table 7, the model terms associated with the flexural strength model were insignificant, with a *p*-value higher than 0.05. Similarly, some model terms in modeling the compressive strength revealed insignificance. But the direct interaction of the PU binder and NS (PU binder × NS) and square of the PU binder were significant in the model, with *p*-values of 0.0106 and 0.0017, respectively, demonstrating a significant *p*-value less than 0.05. The model’s equations for the observed values of all responses of PU-cement mortar modified with NS are expressed in Equations (6) and (7). In the model equations preceding the terms, the synergistic impact of independent parameters on the responses is indicated by negative and positive signs.

$$f_t = +14.04 - 0.445PU + 0.585NS - 0.825PU * NS - 0.865PU^2 - 0.464NS^2 + 0.355PU^2 * NS - 0.51PU * NS^2 \tag{6}$$

$$f_c = +50.75 - 7.4PU + 1.15NS - 2.78PU * NS - 9.69PU^2 - 0.983NS^2 + 4.2PU^2 * NS + 4.61PU * NS^2 \tag{7}$$

where *f_t*, and *f_c* are the flexural strength (MPa), and compressive strength (MPa), respectively. *PU* is the polyurethane binder (%), and *NS* is the Nano silica (%).

Table 6. Analysis of variance of the models.

Response	Variable	Sum of Squares	DF	Mean Square	F-Value	<i>p</i> -Value	Significant
Flexural strength	Model	15.09	7	2.16	5.04	0.0468	significant
	PU binder	0.3961	1	0.3961	0.9270	0.3799	
	NS	0.6845	1	0.6845	1.60	0.2614	
	PU binder × NS	2.72	1	2.72	6.37	0.0529	
	PU binder ²	2.06	1	2.06	4.83	0.0793	
	NS ²	0.5963	1	0.5963	1.40	0.2906	
Compressive strength	Model	618.80	7	88.40	12.75	0.0064	significant
	PU binder	109.52	1	109.52	15.80	0.0106	
	NS	2.64	1	2.64	0.3815	0.5639	
	PU Binder × NS	31.02	1	31.02	4.47	0.0880	
	PU binder ²	259.48	1	259.48	37.42	0.0017	
	NS ²	2.67	1	2.67	0.3847	0.5623	
	PU ² × NS	23.52	1	23.52	3.39	0.1249	
	PU × NS ²	28.40	1	28.40	4.10	0.0989	

Table 7. Statistical indicators and model verification.

Response	R ²	Adj. R ²	Pred. R ²	Mean	Std. Dev.	COV. (%)	AP
Flexural strength	0.8760	0.7023	0.6413	13.43	0.6536	4.87	7.3913
Compressive strength	0.9469	0.8727	5.1647	45.87	2.63	5.75	8.3932

The statistical indicators utilized to evaluate the performance of the developed models are summarized in Table 7, which is sufficient to assess the model’s effectiveness in evaluating the responses and reflecting the goodness-of-fit criteria. The proposed model achieved the model’s precision level with statistical indicators. The outcome revealed that the CCD/RSM model is capable of handling models with a large number of free features, and the mechanical strength was estimated with high accuracy (refer to Table 7); the corresponding scatter plots are shown in Figure 9. The responses (flexural and compressive

strength) were estimated with high accuracy. Additionally, the compressive strength model showed the highest performance with a value $R^2 = 0.9469$. The standard deviation values can be considered when evaluating the models' performance concerning datasets obtained from experimental studies. The models' mean values were compared to standard deviation values to determine how accurately the data fit the developed models. Furthermore, adequate precision (AP) value was needed with the appropriate signal as achieved from the developed model were greater than 4. As a result, the established models might be used to explore the design space as specified in CCD [57]. Moreover, the model's performance was assessed using the coefficient of variation, which reflects the scattering of the data. The models' COV results of 4.87% and 5.75% demonstrated that the scattering in the dataset is insignificant.

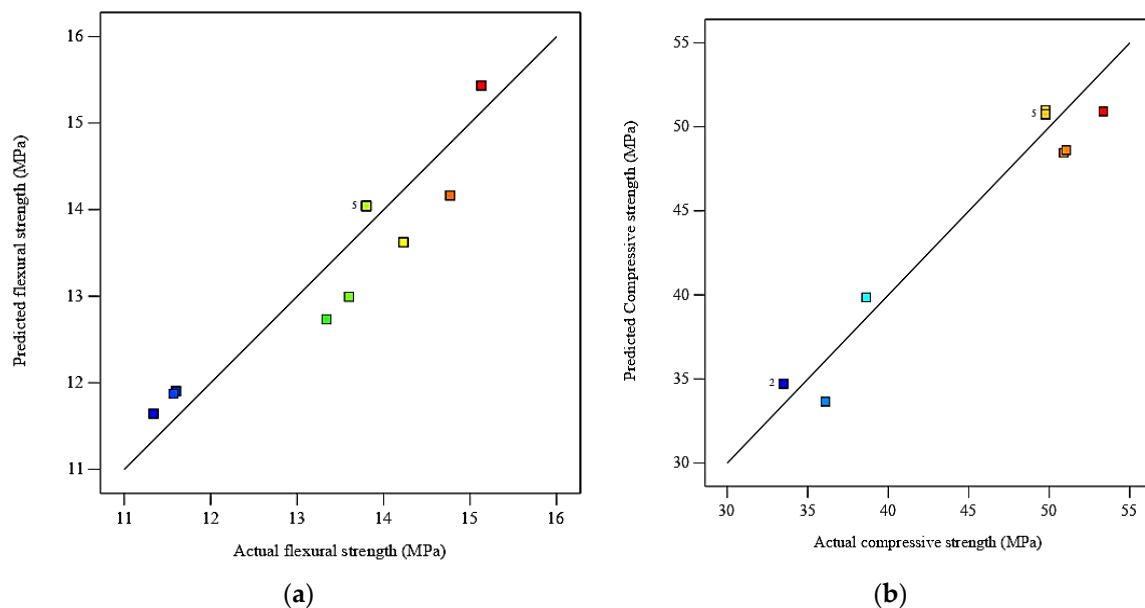


Figure 9. Relationship between actual and predicted values using CCD/RSM model for (a) flexural strength and (b) compressive strength.

Figures 10 and 11 illustrate the dataset of the established model for 3D and 2D response surface plots showing the relationship among the input parameters against the responses. The surface plots also clearly noted the reinforcing effect of PU binder and NS on the cement mortar. As depicted in Figure 10, the flexural and compressive strength increases with the increase in NS, and the peak strengths were obtained by adding 3% NS (the red color portion in the plot). The strength improvement was promoted by adding 10 to 15% PU binders, and then the strengths tended to decline with a further increasing PU binder content, as revealed against 25% PU binders (the blue color portion). From Figure 10a, it can be observed that the mitigating effect of NS is more pronounced in the flexural strength compared with compressive strength, which showed a flatter convex curve. The modeling result agreed with the experimental result regarding the mechanical properties of cement mortar due to the combined effect of the PU binder and NS. The 2D response surface plots of the strength of the PUCM are shown in Figure 11. The plots also reveal the combined effect of the polymer material and NS with optimum PU binder content of 10 to 15%.

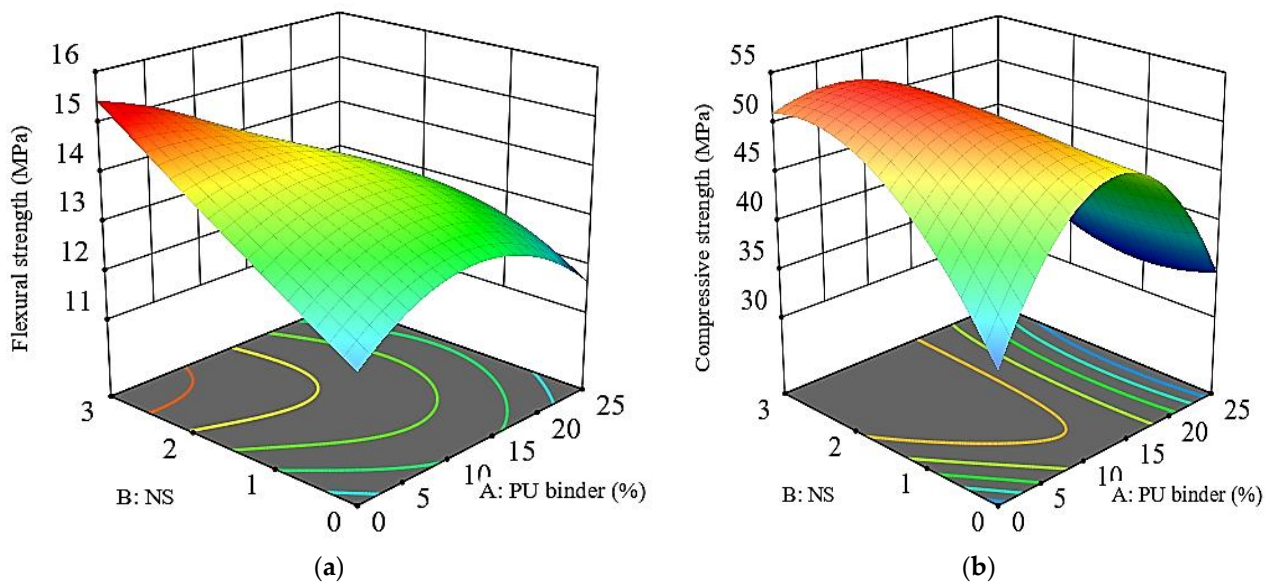


Figure 10. Three-dimensional plots for the simultaneous effect of PU binder and NS in the PUCM for: (a) Flexural strength and (b) compressive strength.

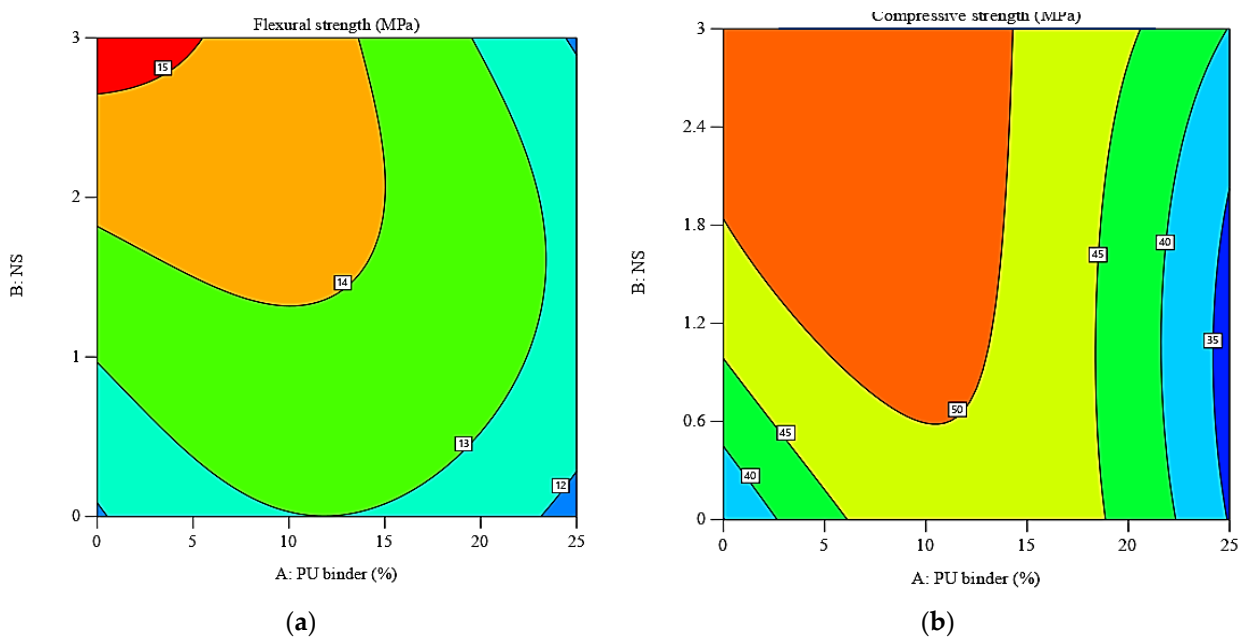


Figure 11. Two-dimensional plots for the simultaneous effect of PU binder and NS in the PUCM for (a) flexural strength and (b) compressive strength.

3.3.2. Optimization of the PUCM Mixtures

The optimization method aims to explore the correct proportion of independent parameters (PU binder and NS) suitable for achieving an optimized PUCM mixture, agreeing to peak values in relation to mechanical strength. The variables were adjusted to a specific range during the optimization method to account for all possible result combinations, and responses were maximized, as listed in Table 8. The solution revealing maximum desirability was considered as the optimal PU–cement mortar mixture, as listed in Table 8, and the optimized strength is depicted in Figure 12. The optimized PUCM mixture was achieved by adding 3.5% PU binder and the addition of 2.93 NS particles by weight of cement. The peak response values were 15.13 MPa and 52.21 MPa for flexural strength and

compressive strength, respectively, with 97.1% of the overall desirability of independent variables, as shown in Table 9.

Table 8. Evaluation criteria for optimization process.

Variables	Symbol	Goal	Lower Limit	Upper Limit
PU binder (%)	PU	In range	0	25
Nano silica (%)	NS	In range	0	3
Flexural strength (MPa)	f_t	Maximize	11.34	15.13
Compressive strength (MPa)	f_c	Maximize	33.5	53.36

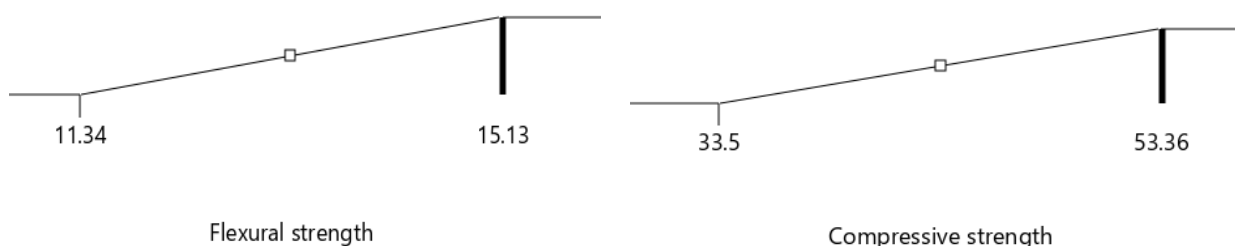


Figure 12. Optimized mechanical properties of PU–cement mortar.

Table 9. Optimized PU–cement mortar mixture.

PU Binder (%)	NS (%)	Flexural Strength (MPa)	Compressive Strength (MPa)	Desirability (%)
3.50	2.93	15.13	52.21	97.1

3.4. Result of AI-Based Model

Sensitivity Analysis of Input Variables

Many studies have popularly used the sensitivity analysis of datasets to treat the inappropriate potential input variable in the modeling task, because utilizing the irrelevant variable in the AI-based model reduces the accuracy of the prediction model and increases the computational demand [58]. Therefore, the Pearson correlation matrix was used in this study to determine the most sensitive variables from the experimental datasets, as depicted in Figure 13. The parameter relevance decreases as it become closer to zero and increases to unity (−1 or +1). The unity values translate the perfect variable. The +ve and −ve values demonstrate a direct and inverse relationship between the independent and dependent parameters. As shown in Figure 14, most input parameters showed a low correlation value with the target parameter. Moreover, an inverse relationship existed between flowability and target parameter, and compressive strength appeared to be the most sensitive parameter for predicting the flexural of the PU–cement mortar with a PC value of 4. The low correlation value between all input and target parameters is attributed to the abnormal distribution of the datasets. The descriptive statistical feature of the input and output parameters are summarized in Table 10.

Table 10. The statistical description of the dataset.

Parameters	Description	Symbol	Unit	Max	Min	Mean	STD	Skew.	Kurt.
Input 1	Curing age	C	d	7.00	28	17.04	10.56	−2.05	0.089
Input 2	PU binder content	PU	%	0.00	25.0	13.69	10.31	−1.48	−0.30
Input 3	Compressive strength	f_c	MPa	21.80	71.6	40.61	12.70	−0.65	0.636
Input 4	Flow ability	F	mm	90.00	230	178.6	61.68	−1.41	−0.74
Output	Flexural strength	f_t	Mpa	8.400	15.9	12.13	1.833	−0.98	0.001

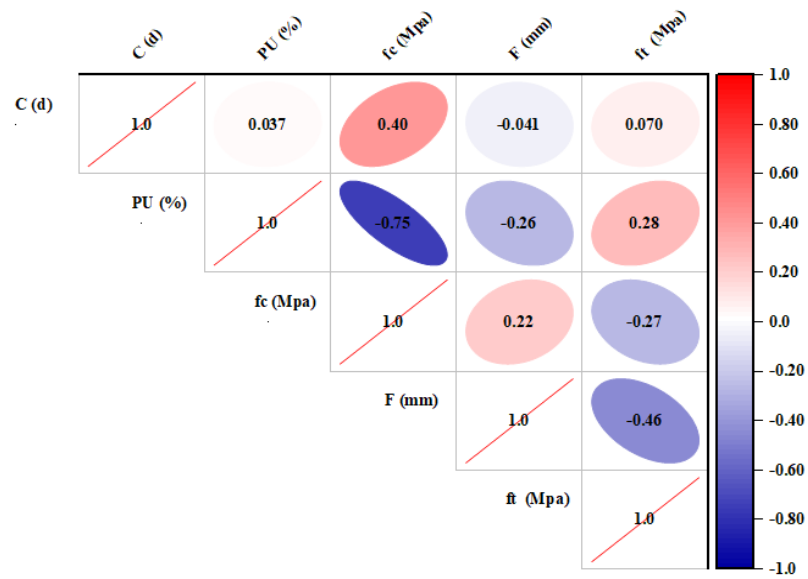


Figure 13. Pearson correlation matrix.

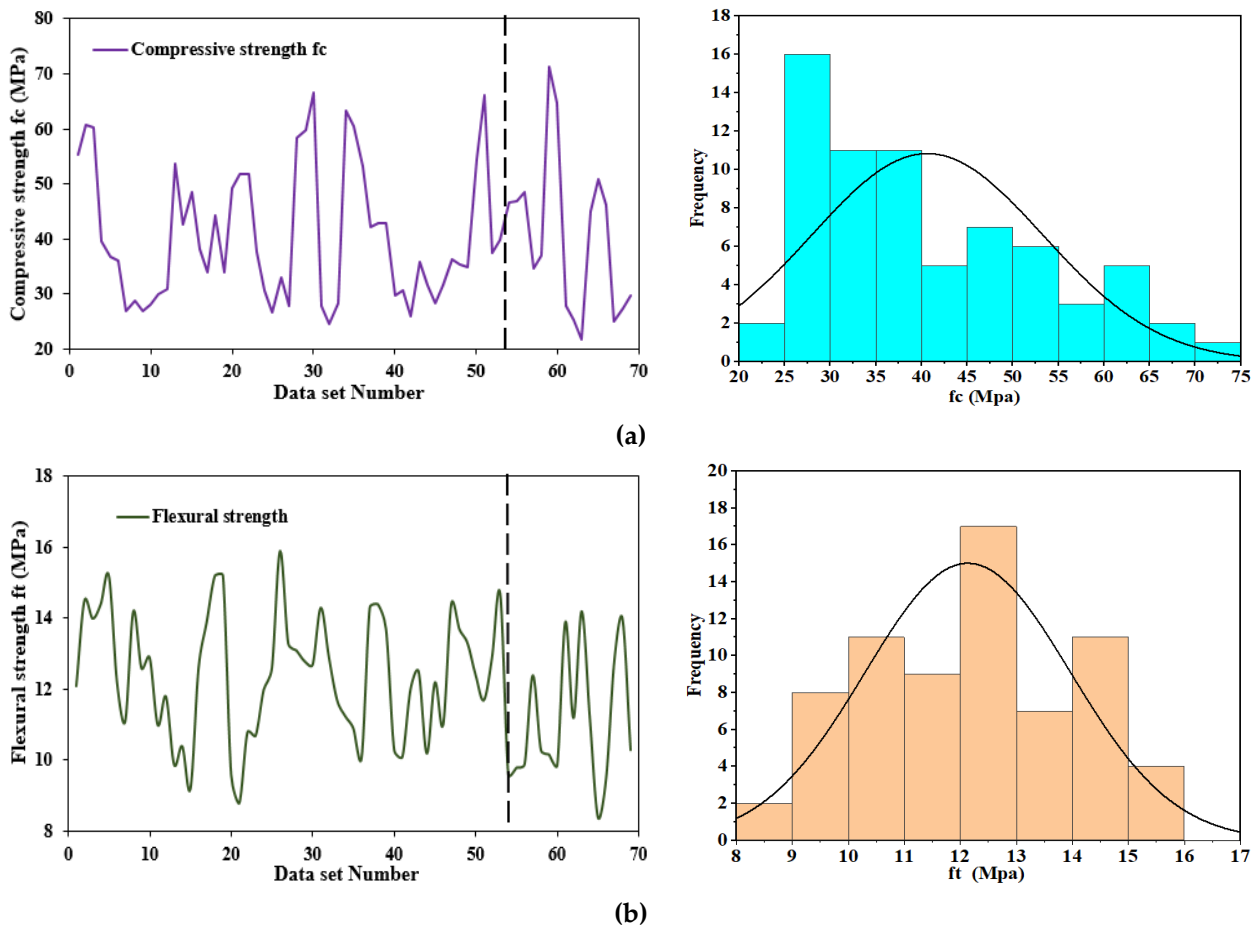


Figure 14. Variation in and frequency distribution of (a) compressive strength and (b) flexural strength.

The variation and distribution in the strength of the most sensitive parameter and target parameter in the modeling task are depicted in Figure 14. As noted in Figure 14a,b, the flexural and compressive strength nearly follow normal distribution. Most of the datasets are within the superimposed curve, and the mean values are concentrated at the center of the curve, particularly for flexural strength data shown in Figure 14b, which reflect

the lesser variation in the flexural strength dataset. The training data and testing data was separated with vertical dotted line, shown on the left side of Figure 14a,b.

Figure 15 presented an agreement plot between the measured and predicted flexural strength from ANN and GPR. It can be observed that predicted values using the GPR model lie closer to the line with minimum deviation than the ANN model. The GPR model achieved a higher coefficient of determination R^2 values = 0.928 and 0.896 in the training and testing phase than the ANN model, with 0.761 and 0.749. Similarly, the GPR model has the lowest MSE, RMSE, and MAE values in both train and testing phases than the ANN model (see Table 11), indicating that the GPR model outperformed ANN in predicting flexural strength in both the training and testing phases.

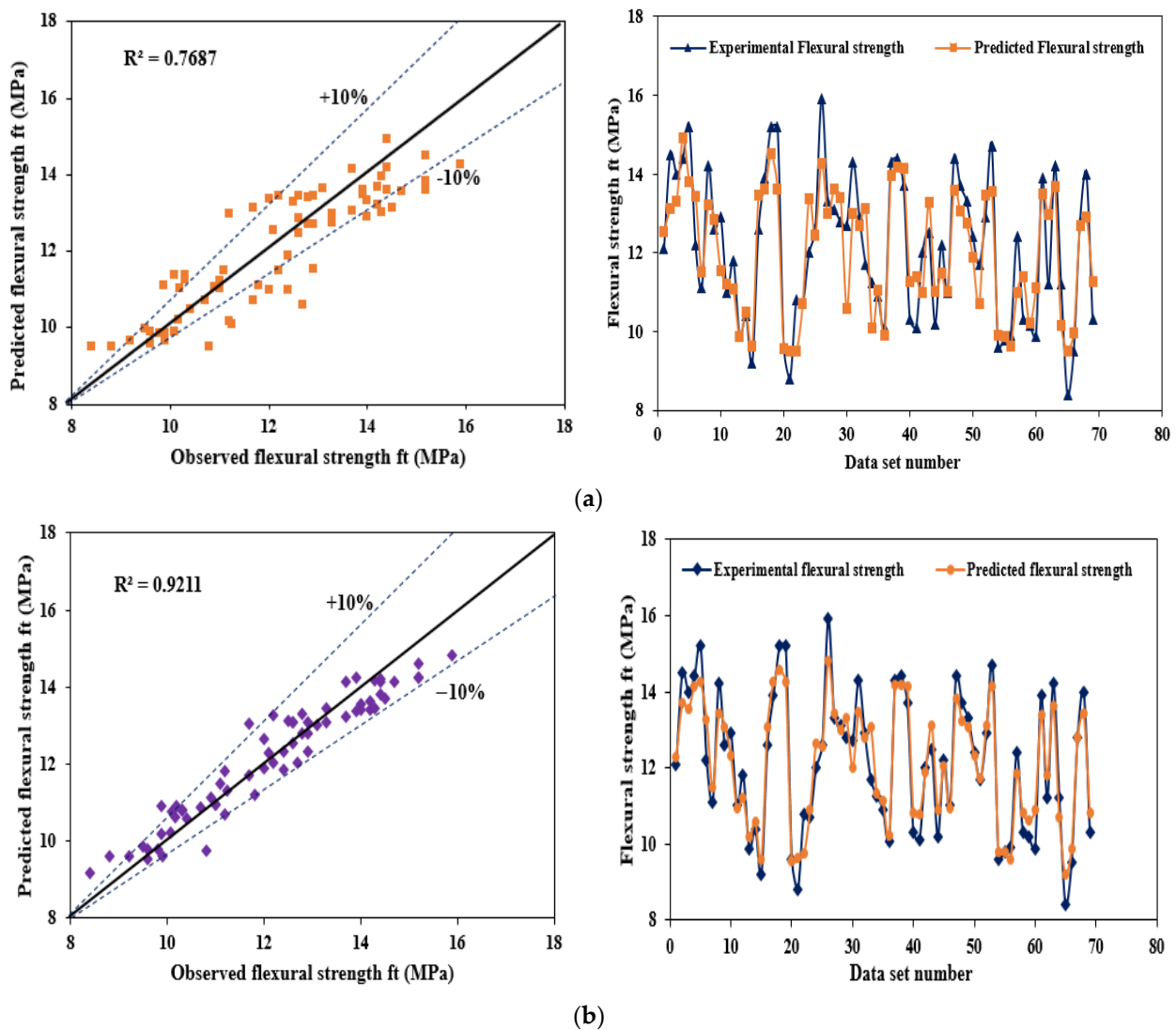


Figure 15. Scatter plot between the experimental and predicted flexural strength for (a) ANN and (b) GPR.

Table 11. Performance evaluation matrices.

Model	Training			R^2	Testing			
	MSE	RMSE	MAE		MSE	RMSE	MAE	R^2
ANN	0.775	0.880	0.744	0.761	0.785	0.886	0.723	0.749
GPR	0.237	0.487	0.411	0.938	0.316	0.562	0.451	0.895

A Taylor diagram and box plot are presented in Figure 16 to compare the performance of the two models better. Taylor plots were used to show the prediction accuracy of the GPR and ANN models in a schematic approach. Three statistical parameters, including the correlation coefficient, RMSE, and standard deviations, were used to evaluate the degree of compliance among the actual and predicted flexural strength. The Taylor diagram (Figure 16a) shows that the GPR model has higher correlation and lower RMSE values than ANN, which confirms that the GPR model performs better than the ANN model.

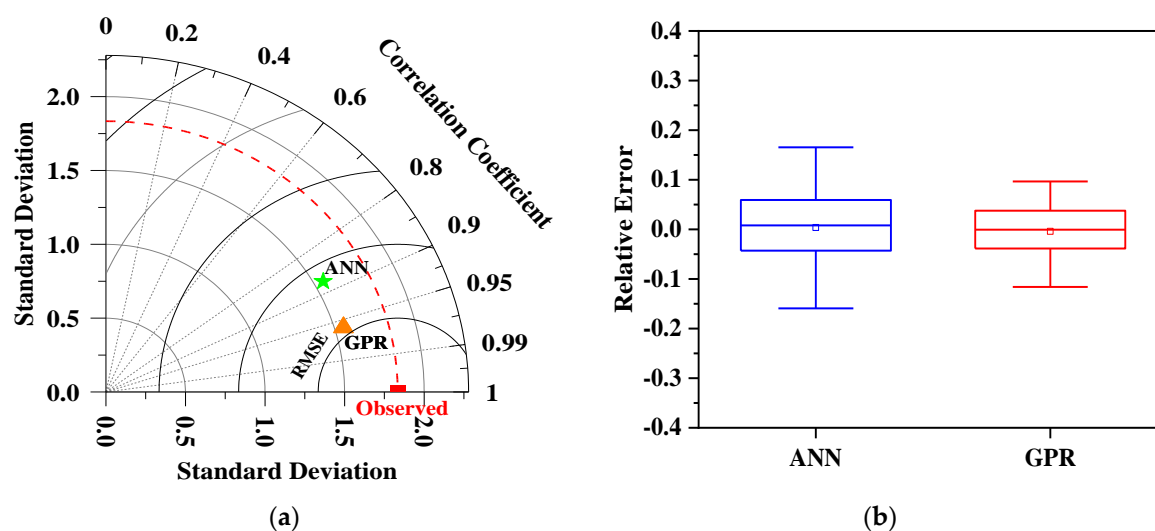


Figure 16. (a) Taylor diagram and (b) box plots.

Figure 16b presents a box plot in which the distribution of relative error of the two models is presented for the two models. The value of the minimum, median, and maximum error, and first quartile and third quartile, were the features used to judge the two models performance. The lower quartile (Q_{25}) value of the ANN model was -0.0456 , and the upper quartile (Q_{75}) value was 0.552 , which was higher when compared with the GPR model where (Q_{25}) and (Q_{75}) is -0.0358 and 0.0395 , respectively. The minimum and maximum error of the ANN was -0.163 and 0.175 , and the GPR model was -0.126 and 0.1400 , respectively, which shows the capacity of the GPR to predict the flexural strength compared to the ANN model.

4. Conclusions

In this study, PUCM was modified with the level of NS particles and tested for mechanical properties tests. Response surface methodology and machine learning algorithms were employed to optimize and model the cement mortar mixtures. The fresh and mechanical properties were used to train the machine learning algorithms, which included artificial neural networks and Gaussian process regression. Four performance indicators assessed the prediction accuracy of the developed. The conclusions outlined in this study are stated below:

1. The mechanical properties of PUCM remarkably decreased with increases in PU binder content, more pronounced in the compressive strength values. However, some part of the lost strength was mitigated due to the reinforcing effect of NS particles. The compressive strength of the PUCM25-0 specimen was 31.34 MPa, which appeared to be the lowest strength among all the mixes.
2. The RSM/CCD developed models evaluated the mechanical properties of PUCM, involving the PU binder and NS material as the independent variable with high accuracy, with R^2 values of 0.8760 and 0.9469 for the flexural and compressive strength, respectively. The optimized PUCM mixture can be achieved by introducing 3.5% PU binder and 2.93% NS particles by weight of cement.

3. Artificial intelligence models were developed to predict the flexural strength of the PUCM. The performance of the machine learning algorithms was tested using performance indicators such as R^2 , MAE, MSE, and RMSE. The GPR algorithm outperformed the ANN with higher R^2 and lower MAE values in the training and testing phases. The GPR can predict flexural strength with 90% accuracy, while ANN can predict it with 75% accuracy. The Taylor diagram and box plots also confirmed that GPR outperforms the ANN model.
4. The macro properties of the polyurethane–cement mortar were explored extensively. However, the finding showed that polyurethane binder significantly affected the mechanical properties of the cementitious-based composite, particularly compressive strength. Therefore, the mechanism development behind these behaviors and how the PU binder affects the reaction kinetics are essential, and may likely change the microstructure of cement mortar, something which has not been explained. Thus, this requires future research.

Author Contributions: H.Z. and Y.E.I.: conceptualization, investigation, supervision, resources, project administration, funding acquisition M.S.M.A.-k. and S.I.H.: conceptualization, methodology, investigation, data curation, writing—original draft, writing—review and editing, visualization. formal analysis, S.S.M.A.-q.: data curation, writing—original draft, writing—review and editing. All authors have read and agreed to the published version of the manuscript.

Funding: This research was funded by Natural Science Foundation of China (No. 51708314) and the APC was funded by the Structures and Materials Laboratory (S&M Lab) of the College of Engineering, Prince Sultan University, Riyadh, Saudi Arabia.

Institutional Review Board Statement: Not applicable.

Informed Consent Statement: Not applicable.

Data Availability Statement: Data available on request due to privacy reasons.

Conflicts of Interest: The authors declare no conflict of interest.

References

1. Zhou, X.; Xie, Y.; Long, G.; Zeng, X.; Li, J.; Yao, L.; Jiang, W.; Pan, Z. DEM analysis of the effect of interface transition zone on dynamic splitting tensile behavior of high-strength concrete based on multi-phase model. *Cem. Concr. Res.* **2021**, *149*, 106577. [[CrossRef](#)]
2. Gao, Y.; Romero, P.; Zhang, H.; Huang, M.; Lai, F. Unsaturated polyester resin concrete: A review. *Constr. Build. Mater.* **2019**, *228*, 116709. [[CrossRef](#)]
3. Verdolotti, L.; Lavoragna, M.; Di Maio, E.; Iannace, S. Hydration-induced reinforcement of rigid polyurethane-cement foams: The effect of the co-continuous morphology on the thermal-oxidative stability. *Polym. Degrad. Stab.* **2013**, *98*, 64–72. [[CrossRef](#)]
4. Sanches, A.O.; Teixeira, G.F.; Zaghet, M.A.; Longo, E.; Malmonge, J.A.; Silva, M.J.; Sakamoto, W.K. Influence of polymer insertion on the dielectric, piezoelectric and acoustic properties of 1-0-3 polyurethane/cement-based piezo composite. *Mater. Res. Bull.* **2019**, *119*, 110541. [[CrossRef](#)]
5. Hussain, H.K.; Liu, G.W.; Yong, Y.W. Experimental study to investigate mechanical properties of new material polyurethane–cement composite (PUC). *Constr. Build. Mater.* **2014**, *50*, 200–208. [[CrossRef](#)]
6. Al-kahtani, M.S.M.; Zhu, H.; Ibrahim, Y.E.; Haruna, S.I. Experimental study on the strength and durability-related properties of ordinary Portland and rapid hardening Portland cement mortar containing polyurethane binder. *Case Stud. Constr. Mater.* **2022**, *17*, e01530. [[CrossRef](#)]
7. Haruna, S.I.; Zhu, H.; Ibrahim, Y.E.; Shao, J.; Adamu, M.; Ahmed, O.S. Impact resistance and flexural behavior of U-shaped concrete specimen retrofitted with polyurethane grout. *Case Stud. Constr. Mater.* **2023**, *19*, e02547. [[CrossRef](#)]
8. Karbhari, V.M.; Eckel, D.A.; Tunis, G.C., III. Strengthening of concrete column stubs through resin infused composite wraps. *J. Thermoplast. Compos. Mater.* **1993**, *6*, 92–107. [[CrossRef](#)]
9. Reis, J.M.L.; Ferreira, A.J.M. Assessment of fracture properties of epoxy polymer concrete reinforced with short carbon and glass fibers. *Constr. Build. Mater.* **2004**, *18*, 523–528. [[CrossRef](#)]
10. Shao, J.; Zhu, H.; Zuo, X.; Lei, W.; Mirgan, S.; Liang, J.; Duan, F. Effect of waste rubber particles on the mechanical performance and deformation properties of epoxy concrete for repair. *Constr. Build. Mater.* **2020**, *241*, 118008. [[CrossRef](#)]
11. Afzal, A.; Kausar, A.; Siddiq, M. Role of polymeric composite in civil engineering applications: A review. *Polym. Technol. Mater.* **2020**, *59*, 1023–1040. [[CrossRef](#)]

12. Ibrahim Haruna, S.; Zhu, H.; Jiang, W.; Shao, J. Evaluation of impact resistance properties of polyurethane-based polymer concrete for the repair of runway subjected to repeated drop-weight impact test. *Constr. Build. Mater.* **2021**, *309*, 125152. [[CrossRef](#)]
13. Asyraf, M.R.M.; Khan, T.; Syamsir, A.; Supian, A.B.M. Synthetic and natural fiber-reinforced polymer matrix composites for advanced applications. *Materials* **2022**, *15*, 6030. [[CrossRef](#)] [[PubMed](#)]
14. Huang, H.; Pang, H.; Huang, J.; Zhao, H.; Liao, B. Synthesis and characterization of ground glass fiber reinforced polyurethane-based polymer concrete as a cementitious runway repair material. *Constr. Build. Mater.* **2020**, *242*, 117221. [[CrossRef](#)]
15. Wu, K.; Zhu, H.; Ibrahim, Y.E.; Jiang, W.; Haruna, S.I.; Shao, J.; Adamu, M. Performance evaluation of bond strength and fiber type on the mechanical properties of polyurethane-based polymer mortar. *Case Stud. Constr. Mater.* **2023**, *18*, e02114. [[CrossRef](#)]
16. Sarva, S.S.; Deschanel, S.; Boyce, M.C.; Chen, W. Stress–strain behavior of a polyurea and a polyurethane from low to high strain rates. *Polymer* **2007**, *48*, 2208–2213. [[CrossRef](#)]
17. Gallu, R.; Méchin, F.; Dalmás, F.; Gérard, J.-F.; Perrin, R.; Loup, F. Rheology-morphology relationships of new polymer-modified bitumen based on thermoplastic polyurethanes (TPU). *Constr. Build. Mater.* **2020**, *259*, 120404. [[CrossRef](#)]
18. Grujicic, M.; Pandurangan, B.; He, T.; Cheeseman, B.A.; Yen, C.-F.; Randow, C.L. Computational investigation of impact energy absorption capability of polyurea coatings via deformation-induced glass transition. *Mater. Sci. Eng. A* **2010**, *527*, 7741–7751. [[CrossRef](#)]
19. Li, J.; Zhang, J.; Chen, S. Study on dynamic viscoelastic properties and constitutive model of non-water reacted polyurethane grouting materials. *Measurement* **2021**, *176*, 109115. [[CrossRef](#)]
20. Choi, H.J.; Kim, J.H. Static and dynamic comfort properties of polyurethane foams including a flexible amine crosslinker. *J. Ind. Eng. Chem.* **2020**, *90*, 260–265. [[CrossRef](#)]
21. Mounanga, P.; Gbongbon, W.; Poullain, P.; Turcry, P. Proportioning and characterization of lightweight concrete mixtures made with rigid polyurethane foam wastes. *Cem. Concr. Compos.* **2008**, *30*, 806–814. [[CrossRef](#)]
22. ACI Committee 548. 548.6R-96: *Polymer Concrete-Structural Applications. State-of-the-Art Report*; American Concrete Institute: Farmington Hills, MI, USA, 1996; pp. 1–23.
23. Harith, I.K. Study on polyurethane foamed concrete for use in structural applications. *Case Stud. Constr. Mater.* **2018**, *8*, 79–86. [[CrossRef](#)]
24. Jia, Z.; Jia, D.; Sun, Q.; Wang, Y.; Ding, H. Preparation and mechanical-fatigue properties of elastic polyurethane concrete composites. *Materials* **2021**, *14*, 3839. [[CrossRef](#)] [[PubMed](#)]
25. Nikoukalam, M.T.; Sideris, P. Experimental characterization and constitutive modeling of polyurethanes for structural applications, accounting for damage, hysteresis, loading rate and long term effects. *Eng. Struct.* **2019**, *198*, 109462. [[CrossRef](#)]
26. Tang, J.; Liu, J.; Yu, C.; Wang, R. Influence of cationic polyurethane on mechanical properties of cement based materials and its hydration mechanism. *Constr. Build. Mater.* **2017**, *137*, 494–504. [[CrossRef](#)]
27. Chen, X.; Zhou, N.; Zhang, H. In-Situ polymerization and characterization of poly (ϵ -caprolactone) urethane/SiO₂ nanocomposites. *J. Phys. Conf. Ser.* **2009**, *188*, 012025. [[CrossRef](#)]
28. Alshahrani, H.; Sebaey, T.A.; Awd Allah, M.M.; Abd El-baky, M.A. Multi-response optimization of crashworthy performance of perforated thin walled tubes. *J. Compos. Mater.* **2023**, *57*, 1579–1597. [[CrossRef](#)]
29. Abba, S.I.; Elkiran, G. Effluent prediction of chemical oxygen demand from the astewater treatment plant using artificial neural network application. *Procedia Comput. Sci.* **2017**, *120*, 156–163. [[CrossRef](#)]
30. Haruna, S.I.; Malami, S.I.; Adamu, M.; Usman, A.G.; Farouq, A.I.B.; Ali, S.I.A.; Abba, S.I. Compressive Strength of Self-Compacting Concrete Modified with Rice Husk Ash and Calcium Carbide Waste Modeling: A Feasibility of Emerging Emotional Intelligent Model (EANN) versus Traditional FFNN. *Arab. J. Sci. Eng.* **2021**, *46*, 11207–11222. [[CrossRef](#)]
31. Abba, S.I.; Benaafi, M.; Usman, A.G.; Aljundi, I.H. Sandstone groundwater salinization modelling using physicochemical variables in Southern Saudi Arabia: Application of novel data intelligent algorithms. *Ain Shams Eng. J.* **2023**, *14*, 101894. [[CrossRef](#)]
32. Adamu, M.; Haruna, S.I.; Malami, S.I.; Ibrahim, M.N.; Abba, S.I.; Ibrahim, Y.E. Prediction of compressive strength of concrete incorporated with jujube seed as partial replacement of coarse aggregate: A feasibility of Hammerstein–Wiener model versus support vector machine. *Model. Earth Syst. Environ.* **2022**, *8*, 3435–3445. [[CrossRef](#)]
33. Ehsani, M.; Moghadas Nejad, F.; Hajikarimi, P. Developing an optimized faulting prediction model in Jointed Plain Concrete Pavement using artificial neural networks and random forest methods. *Int. J. Pavement Eng.* **2022**, *24*, 2057975. [[CrossRef](#)]
34. Lee, T.-S.; Chiu, C.-C.; Chou, Y.-C.; Lu, C.-J. Mining the customer credit using classification and regression tree and multivariate adaptive regression splines. *Comput. Stat. Data Anal.* **2006**, *50*, 1113–1130. [[CrossRef](#)]
35. Chou, J.-S.; Tsai, C.-F. Concrete compressive strength analysis using a combined classification and regression technique. *Autom. Constr.* **2012**, *24*, 52–60. [[CrossRef](#)]
36. Kooshkaki, A.; Eskandari-Naddaf, H. Effect of porosity on predicting compressive and flexural strength of cement mortar containing micro and nano-silica by multi-objective ANN modeling. *Constr. Build. Mater.* **2019**, *212*, 176–191. [[CrossRef](#)]
37. Ahmad, A.; Ostrowski, K.A.; Mašlak, M.; Farooq, F.; Mehmood, I.; Nafees, A. Comparative Study of Supervised Machine Learning Algorithms for Predicting the Compressive Strength of Concrete at High Temperature. *Mater.* **2021**, *14*, 4222. [[CrossRef](#)] [[PubMed](#)]
38. Rupasinghe, M.; Mendis, P.; Ngo, T.; Nguyen, T.N.; Sofi, M. Compressive strength prediction of nano-silica incorporated cement systems based on a multiscale approach. *Mater. Des.* **2017**, *115*, 379–392. [[CrossRef](#)]
39. Gao, H.; Sun, Q. Study on Fatigue Test and Life Prediction of Polyurethane Cement Composite (PUC) under High or Low Temperature Conditions. *Adv. Mater. Sci. Eng.* **2020**, *2020*, 2398064. [[CrossRef](#)]

40. Diaconescu, R.-M.; Barbuta, M.; Harja, M. Prediction of properties of polymer concrete composite with tire rubber using neural networks. *Mater. Sci. Eng. B* **2013**, *178*, 1259–1267. [[CrossRef](#)]
41. Marinela, B.; Rodica-Mariana, D.; Maria, H. Using Neural Networks for Prediction of Properties of Polymer Concrete with Fly Ash. *J. Mater. Civ. Eng.* **2012**, *24*, 523–528. [[CrossRef](#)]
42. Unnikrishna Pillai, U.; Anand, K.B. Performance evaluation of polyurethane-nano silica modified cement mortar. *Mater. Today Proc.* **2021**, *46*, 4788–4794. [[CrossRef](#)]
43. Barbhuiya, G.H.; Moiz, M.A.; Hasan, S.D.; Zaheer, M.M. Effects of the nanosilica addition on cement concrete: A review. *Mater. Today Proc.* **2020**, *32*, 560–566. [[CrossRef](#)]
44. Li, M.; Sun, J.; Li, L.; Meng, L.; Wang, S.; Wei, J.; Mao, J. Effect of nanosilica on fiber pullout behavior and mechanical properties of strain hardening ultra-high performance concrete. *Constr. Build. Mater.* **2023**, *367*, 130255. [[CrossRef](#)]
45. Demir, M.M.; Yilgor, I.; Yilgor, E.; Erman, B. Electrospinning of polyurethane fibers. *Polymer* **2002**, *43*, 3303–3309. [[CrossRef](#)]
46. DL/T5126-2001; Test Code on Polymer-Modified Cement Mortar. National Standard of China: Beijing, China, 2001.
47. Montgomery, D.C. *Design and Analysis of Experiments*; John Wiley & Sons: Hoboken, NJ, USA, 2017.
48. Ghaffari, A.; Abdollahi, H.; Khoshayand, M.; Bozchalooi, I.; Dadgar, A.; Rafiee-Tehrani, M. Performance comparison of neural network training algorithms in modeling of bimodal drug delivery. *Int. J. Pharm.* **2006**, *327*, 126–138. [[CrossRef](#)] [[PubMed](#)]
49. Ibrahim Bibi Farouk, A.; Zhu, J.; Ding, J.; Haruna, S.I. Prediction and uncertainty quantification of ultimate bond strength between UHPC and reinforcing steel bar using a hybrid machine learning approach. *Constr. Build. Mater.* **2022**, *345*, 128360. [[CrossRef](#)]
50. Omran, B.A.; Chen, Q.; Jin, R. Comparison of data mining techniques for predicting compressive strength of environmentally friendly concrete. *J. Comput. Civ. Eng.* **2016**, *30*, 4016029. [[CrossRef](#)]
51. Cheng, M.-Y.; Huang, C.-C.; Roy, A.F. Van Predicting project success in construction using an evolutionary Gaussian process inference model. *J. Civ. Eng. Manag.* **2013**, *19*, S202–S211. [[CrossRef](#)]
52. Pal, M.; Deswal, S. Modelling pile capacity using Gaussian process regression. *Comput. Geotech.* **2010**, *37*, 942–947. [[CrossRef](#)]
53. Williams, C.K.; Rasmussen, C.E. *Gaussian Processes for Machine Learning*; MIT Press: Cambridge, MA, USA, 2006.
54. Gouda, S.G.; Hussein, Z.; Luo, S.; Yuan, Q. Model selection for accurate daily global solar radiation prediction in China. *J. Clean. Prod.* **2019**, *221*, 132–144. [[CrossRef](#)]
55. Farouk, A.I.B.; Jinsong, Z. Prediction of Interface Bond Strength Between Ultra-High-Performance Concrete (UHPC) and Normal Strength Concrete (NSC) Using a Machine Learning Approach. *Arab. J. Sci. Eng.* **2022**, *47*, 5337–5363. [[CrossRef](#)]
56. Haruna, S.I.; Ibrahim, Y.E.; Han, Z.; Farouk, A.I.B. Flexural Response of Concrete Specimen Retrofitted with PU Grout Material: Experimental and Numerical Modeling. *Polymers* **2023**, *15*, 4114. [[CrossRef](#)] [[PubMed](#)]
57. Adamu, M.; Mohammed, B.S.; Shahir Liew, M. Mechanical properties and performance of high volume fly ash roller compacted concrete containing crumb rubber and nano silica. *Constr. Build. Mater.* **2018**, *171*, 521–538. [[CrossRef](#)]
58. Nourani, V.; Sharghi, Z.A.E. Sensitivity analysis and ensemble artificial intelligence-based model for short-term prediction of NO₂ concentration. *Int. J. Environ. Sci. Technol.* **2021**, *18*, 2703–2722. [[CrossRef](#)]

Disclaimer/Publisher's Note: The statements, opinions and data contained in all publications are solely those of the individual author(s) and contributor(s) and not of MDPI and/or the editor(s). MDPI and/or the editor(s) disclaim responsibility for any injury to people or property resulting from any ideas, methods, instructions or products referred to in the content.